Effects of Applying Brand-New Designs on the Performance of PEM Fuel Cell and Water Flooding Phenomena

Samanpour, Hossein
Mechanical Engineering Department, Urmia University, Urmia, I.R. IRAN

Ahmadi, Nima*[+•]
Department of Mechanical Engineering, Technical and Vocational University (TVU), Tehran, I.R. IRAN
Jabbary, Ali
Mechanical Engineering Department, Urmia University, Urmia, I.R. IRAN

ABSTRACT: *Numerous researchers use numerical simulations to precisely recognize the processes before mass production to provide a basic model for optimizing the fuel cell. In this study, we presented brand-new designs for cylindrical PEMFCs in the Three-Dimensional form. We used the Finite Volume Method to simulate the fuel cell processes and established a genuine correspondence between our simulation results and valid outcomes. We introduced innovative designs to increase the performance of cylindrical polymer fuel cells. Then, we examined the effects of progressive developments in cross-section design, the fuel cell structure, the output current densities, and, eventually, the flooding phenomenon. The results revealed the optimum capacity of the cylindrical fuel cell compared with an elliptical cross-section. Due to more extensive transport zones and pressure drop effects, we need to find the optimum cell capacity to pass the reactive regions.*

KEYWORDS: *PEMFC; Finite Volume Method (FVM); Flooding phenomena; Three-dimensional.*

INTRODUCTION

Modern energy-converting devices, known as Proton Exchange Membrane Fuel Cells (PEMFC), have taken lot of attention. Industries such as transformational systems and energy enterprises are widely using PEMFCs. The advantages of using PEMFC are;

- Higher performance,
- Low-temperature operations,
- Fast start-ups.
- Noiseless procedure,
- Non-pollutant activity,

Despite their advantages, these types of fuel cells need performance optimizations, and they should be economically viable to enter a safe competition with the former energy industry [1-4]. Several studies carried out on fuel cells, yet extreme expenses limit the fuel cell industry to be a reliable trading product. It uses

***** *To whom correspondence should be addressed.*
+ *E-mail: ima.ahmadi.eng@gmail.com*
● *Other Address: Tallinn University of Technology, School of Maritime Academy, Tallinna 19, Kuressaare, ESTONIA*
1021-9986/2022/2/618-634 *17/$/6.07*

hydrogen as a fuel and oxygen-air mixture as the oxidizer to produce electricity. Usually, a typical fuel cell progresses with the following instructions: Gas flows into the gas channels, then a catalyst layer makes the oxidation process form hydrogen and oxygen ions. Consequently, protons transport toward the membrane from the anode to the cathode side and combine with oxygen ions at the cathode side to form the water. Eventually, this process generates water along the cathode side, and the amount of water enhances from the inlet to the outlet Electrons transfer from an external circuit to reach the cathode side. By moving the electrons from the external circuit, electricity will be generated [5-10]. The reaction of reactants respectively at the anode and cathode side is shown as:

$$H_2 \rightarrow 2H^+ + 2e^- \qquad \text{Anode Side}$$

$$O_2 + 2H^+ + 2e^- \rightarrow H_2O \qquad \text{Cathode Side}$$

Cathode and Anode sections have electrically conducted porous media that are produced with carbon. The exterior parts of the electrodes are in contact with the carbon-based polymer electrolyte membrane and catalyst. Anode and cathode have active layers that are the regions in which fuel cell reduction and half-reaction oxidation activities occur. Fuel cell electrodes are covered with a porous structure to allow the gas to flow through the channels and are considerably intended to maximize the surface area per unit volume. The electrodes' capability enables the gas diffusion layer to decrease oxygen and hydrogen transport resistance to active/reactive regions. Many research efforts attend to improve real-life fuel cell simulations [11-14].

Multiple investigations led to optimizing the operation of the PEMFCs. Numerous parameters like temperature, pressure, moisturizing of gas flow, and other geometric parameters can affect the optimal function of the polymer fuel cell. Geometric parameters demand a primary role in controlling the operation of a PEM fuel cell. A fuel cell's performance with a larger width model is less than a lower width model [15-18]. In this approach, the efficacy of geometric parameters on fuel cell maintenance is one of the crucial circumstances. Several studies investigate the effects of both operational parameters and geometric variations of gas diffusion layers on fuel cell performance.

The development of a bump in GDLs results in a significant improvement in fuel cell performance [19]. *Ebrahimi et al.* [20] conducted a relevant study considering two-dimensional and numerical simulations. They investigated the influence of a uniform diffusion of non-homogenous catalyst layers on the fuel cell's performance. This study confirms that the optimal distribution in cathode and anode sections would increase fuel cells' execution by %70. *Cooper et al.* [21] investigated the particle coefficient moderating effect on the PEM fuel cell performance with the inter-connected gas channels. Furthermore, *Yan et al.* [22] simulated mass transfer phenomena in an unsteady state for the PEM fuel cell.

Hence, *Gou et al.* [23] attended a study demonstrating two-dimensional analytical models for the fuel cell. *Ahmadi et al.* [24] applied the perturbation method to present an analytical model for the cylindrical PEM fuel cell. They obtained the velocity distribution in the gas channel. Additionally, they [25] examined and modeled the transport of species in a fuel cell. General fuel cell designs are usually in square-shaped channels. This research intends to investigate geometrical variations affecting the performance of a PEM fuel cell. In this approach, we proposed the fuel cell design by the membrane and electrode assembly. Then we presented a cylindrical fuel cell scheme as a novel design to compare its performance with the base model. In other words, the cross-section of the fuel cell will be changed to a circular and elliptical shape. The transport phenomena and fuel cell performance will be studied in more detail.

THEORETICAL SECTION

Fig. 1 illustrates the computational domain (Left) and the base model's definition of its components (Right). Furthermore, we will mention the appropriate sizes of the elements in **Error! Reference source not found.**.

The cell contains hydrogen and oxygen channels, bipolar plates on the anode and cathode sides, electrodes, and a membrane among gas channels.

Model assumptions

We implemented several modifications in the current research including;

- Non-isothermal design
- Ideal gas existence
- Homogeneous gas diffusion

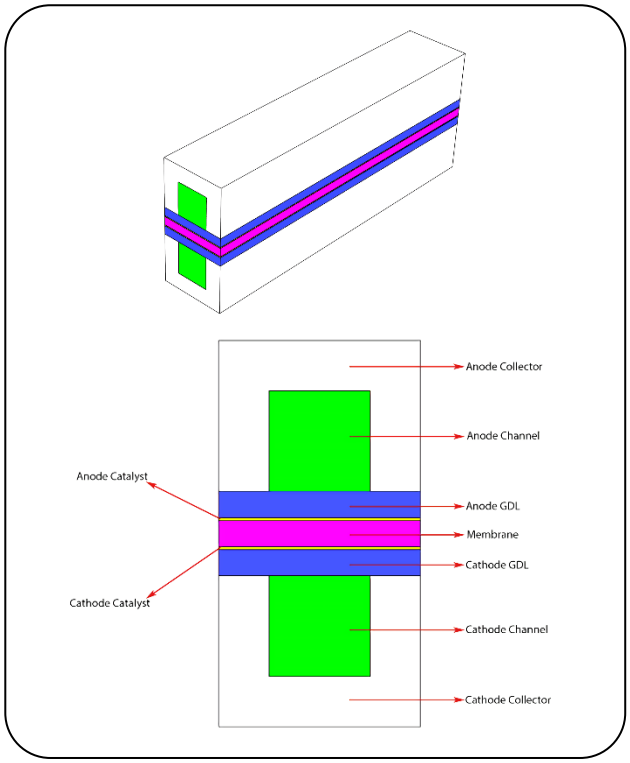

Fig. 1: 3D computational domain's overview of the fuel cell.

- Uniform catalyst layer
- Unstable electrical current
- and the pressure gradient is minimal along with the cell.

Due to these assumptions, the fluid is incompressible, and velocity is moderate.

Governing equations

This numerical simulation consists of the following governing equations that we mentioned below;

$$\nabla \cdot \rho \vec{u} = 0 \tag{1}$$

$$\frac{1}{\epsilon^{eff^2}} \nabla \cdot \left(\rho \vec{u} \vec{u} \right) = -\nabla p + \nabla \cdot \left(\mu \nabla \vec{u} \right) + S_u \tag{2}$$

$$\nabla \cdot \left(\vec{u} C_K \right) = \nabla \cdot \left(D_K^{eff} \nabla C_K \right) + S_K \tag{3}$$

$$\nabla \cdot \left(K_e^{eff} \nabla \Phi_e \right) + S_\Phi = 0 \tag{4}$$

ρ is the gas density. ε^{eff} is the efficient porosity in the interior side of the porous layer. μ notes the gas viscosity in the momentum equation, which illustrates in equation (2). S_u is the momentum source term that applies to illustrate Darcy drag force to move through GDL and catalyst layer [26] which we mentioned below;

$$S_u = -\frac{\mu}{K} \vec{u} \tag{5}$$

In Eq. (5), K stands for the gas permeability inside the porous region. In the Species equation given in Eq. (3), k is the efficient penetration coefficient. Bragman presented Eq. (6) to describe the gas penetration through the porous medium of GDL and CL [27];

$$D_K^{eff} = \left(\epsilon_{eff} \right)^{1.5} D_K \tag{6}$$

Moreover, the diffusion coefficient is a function of pressure and temperature [28];

$$D_K = D_K^0 \left(\frac{T}{T_0} \right)^{\frac{3}{2}} \left(\frac{P_0}{P} \right) \tag{7}$$

We expressed the transport properties of the species in Table.

Eq. (8) represents Maxwell's equation of conductivity. In this equation, K_e demonstrates the ion conductance in the ion-conducting phase. It is published by *Springer*, *Zavadzinsky*, and *Vagathsfield* [29];

$$K_e = \exp\left(1268 \left(\frac{1}{303} - \frac{1}{T_{cell} + 273} \right) \right) \times \left(0.005139\lambda - 0.00326 \right) \qquad (for\ \lambda > 1) \tag{8}$$

Moreover, in Eq. (8), λ is the water molecule numbers in each sulfonate group inside the membrane. The water level considers a function of water activity and designated through experimental data [30];

$$\lambda = 0.3 + 6a\left(1 - \tanh\left(a - 0.5\right)\right) + 3.9\sqrt{a}\left(1 + \tanh\left(\frac{a - 0.89}{0.23}\right)\right) \tag{9}$$

The following equation specifies water activity:

$$a = \frac{C_w R T}{P_w^{sat}} \nabla \tag{10}$$

Bragman's equation represents proton conductance in the catalyst layer [31];

$$K_e^{eff} = \epsilon_m^{1.5} K_e \tag{11}$$

Table 1: Transitional properties of the species [28].

Quantity	Value
$D_{H_2}^0$	$1.1 \times 10^{-4}\ m^2/s$
$D_{O_2}^0$	$3.8 \times 10^{-5}\ m^2/s$
$D_{H_2O}^0$	$7.35 \times 10^{-5}\ m^2/s$
$D_{H_2}^{mem.}$	$8.55 \times 10^{-11}\ m^2/s$
$D_{O_2}^{mem.}$	$1.88 \times 10^{-11}\ m^2/s$

Table 2: Boundary conditions in polymer fuel cell [34].

Region	Boundary condition
Anode channel inlet	$u = u_{in}, \quad T = T_{in}, \quad v = 0, \quad C_{H_2} = C^a_{H_2,in}, \quad C^a_{H_2O,in}$
Cathode channel inlet	$u = u_{in}, \quad T = T_{in}, \quad v = 0, \quad C_{O_2} = C^c_{O_2,in}, \quad C_{N_2} = C^c_{N_2,in}$
The anode and the cathode channel outlet	$\frac{\partial u}{\partial x} = \frac{\partial v}{\partial x} = \frac{\partial w}{\partial z} = \frac{\partial T}{\partial x} = 0$
The interface of gas channels and GDLs	$\frac{\partial u}{\partial y}\|_{y=y_1^-} = \epsilon_{eff,GDL}\frac{\partial u}{\partial y}\|_{y=h_1^+}, \quad \frac{\partial v}{\partial y}\|_{y=h_1^-} = \epsilon_{eff,GDL}\frac{\partial v}{\partial y}\|_{y=h_1^+}$ $\frac{\partial u}{\partial y}\|_{y=h_1^-} = \epsilon_{eff,GDL}\frac{\partial u}{\partial y}\|_{y=h_1^+}, \quad \frac{\partial v}{\partial y}\|_{y=h_1^-} = \epsilon_{eff,GDL}\frac{\partial v}{\partial y}\|_{y=h_1^+}$ $\frac{\partial w}{\partial y}\|_{y=h_1^-} = \epsilon_{eff,GDL}\frac{\partial w}{\partial y}\|_{y=h_1^+}$
The interface of GDLs and CLs	$\epsilon_{eff,GDL}\frac{\partial u}{\partial y}\|_{y=h_2^-} = \epsilon_{eff,CL}\frac{\partial u}{\partial y}\|_{y=h_2^+}, \quad \epsilon_{eff,GDL}\frac{\partial v}{\partial y}\|_{y=h_2^-} = \epsilon_{eff,CL}\frac{\partial v}{\partial y}\|_{y=h_2^+},$ $\epsilon_{eff,GDL}\frac{\partial w}{\partial y}\|_{y=h_2^-} = \epsilon_{eff,CL}\frac{\partial w}{\partial y}\|_{y=h_2^+}$
The interface of CL and membrane	$u = v = w = C_i = 0$
The upper surface of gas channels	$u = v = w = C_i = 0, \quad T_{surface} = 353K$
The lower surface of gas channels	$u = w = 0, \quad T_{surface} = T_{wall}$
The upper surface of anode bipolar plates	$\phi_{sol} = 0, \quad \frac{\partial \phi_{mem}}{\partial y} = 0$
The upper surface of cathode bipolar plates	$\phi_{sol} = V_{cell}, \quad \frac{\partial \phi_{mem}}{\partial y} = 0$
External surfaces	$\frac{\partial \phi_{mem}}{\partial x} = 0, \quad \frac{\partial \phi_{mem}}{\partial z} = 0, \quad \frac{\partial \phi_{sol}}{\partial x} = 0, \quad \frac{\partial \phi_{sol}}{\partial z} = 0$

In Eq. (11), ε_m is the volume fraction of the membrane phase in the catalyst layer. We showed that the applied terms for species are in Eq. (3). The local current density in the membrane is estimated by the following equation [32, 33];

$$I = \kappa_e \nabla \Phi_e \tag{12}$$

Then the average current density is estimated by the following equation;

$$I_{avg} = \frac{1}{A}\int_{A_{mem}} I\, dA \tag{13}$$

In Equation (13), A is the efficient electrode's reaction area.

Boundary conditions and solution methods

Table explains the given boundary conditions in this study; we set the hydrogen and the air-oxygen mix at the inlets of gas channels at the anode and cathode sides, according to the momentum conservation equation. The stoichiometry theory balances the required fuel quantity to achieve the fuel cell's primary assignments.

The gas velocity entering the gas channels is obtainable by the following equations [34];

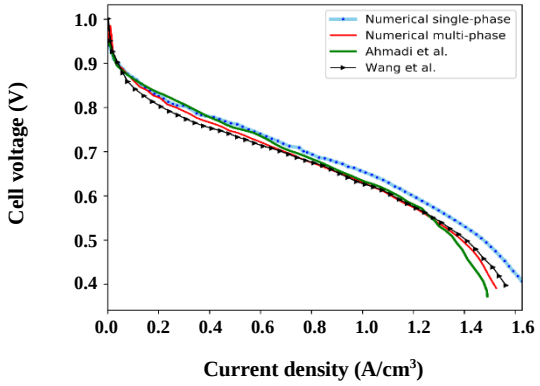

Fig. 2: Validation of Polarization curves of the presented model.

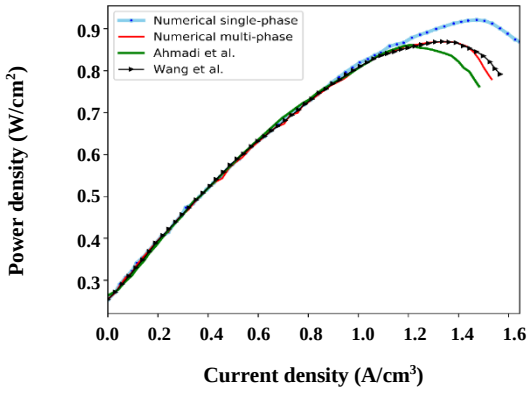

Fig. 3: Validation of power density curves of the presented model.

$$\begin{cases} u_{an} = \dfrac{\zeta}{X_{H2,in}} \dfrac{I_{avg}}{2F} \dfrac{R\,T_{in}}{P_{in}} \dfrac{A_{MEA}}{A_{ch}} \\ u_{cth} = \dfrac{\zeta}{X_{O2,in}} \dfrac{I_{avg}}{4F} \dfrac{R\,T_{in}}{P_{in}} \dfrac{A_{MEA}}{A_{ch}} \end{cases} \quad (14)$$

In the mentioned equation, ζ is the stoichiometry value at both the anode and cathode sides. $X_{H_2,in}$ is the volume fraction of intake hydrogen. I_{avg} is the average reference current density and equals to $I_{avg} = 15000\ A/m^2$. R is global gas constant, F is Faraday constant, T_{in} and P_{in} are the input temperature and pressure in the gas channels, respectively. A_{MEA} is the active area of the fuel cell surface and A_{ch} is the inlet area of the gas channel.

RESULTS AND DISCUSSION

We used CFD methods to obtain precise outcomes of the governing equations presented for the given PEM fuel cell cases [35]. We will discuss these results in the following sections.

Model validation

After applying numerical methods to solve the problem, we compare the results with the experimental data presented by *Wang et al.* and *Ahmadi et al.* [25, 34] to confirm the proposed model's accuracy. In Fig. 2, an acceptable balance between the numerical model and experimental data is observable. We demonstrated the power density curve also for the numerical model. The connection between cell Voltage, current density, and power density is obtainable by $P = V \times I$. A negligible difference was observed in $0.4V$ Voltage in single-phase simulation.

Because the single-phase model is unable to apprehend the effects of liquid water into account, therefore, in these Voltages, the current density cannot be optimally modeled. A multi-phase model performs proper settlement with the experimental results. Consequently, attributing the base model, we investigated the effectiveness of geometrical variations in the fuel cell process. After verifying the base model results, we consider the effects of geometrical changes on the fuel cell's performance.

The validation of power density curves for the given models is noticeable in **Error! Reference source not found.**.

Error! Reference source not found. presents the operational status of the fuel cell and its geometrical parameters. The input gases are in the humid condition approaching the anode and cathode sides.

This study intends to compare the fuel cell with a square-shaped channel and a cylindrical fuel cell. Further, we aim to investigate the effects of geometrical changes on the performance of the fuel cell. Fig. 4 shows the grid network of the base model of the front view.

Fig. 5 denotes the result of a grid independence test. There will be no variation in fuel cell outflow current density if we choose more than 200,000 computational cells. Increasing the number of grid cells won't make any change in results. Consequently, numerical results are independent of the number of cells.

Fig. 6 proves the grid independence test and represents the oxygen molecule fraction and the cathode catalyst layer's length.

Table 3: Geometrical and operational parameters of the cell.

Parameter	Symbol	Value	Unit
Channel length	L	0.05	m
Channel width	W	3×10^{-3}	m
Channel height	H	3×10^{-3}	m
Land area width	W_{land}	3×10^{-3}	m
Gas diffusion layer thickness	d_{GDL}	0.26×10^{-3}	m
Wet membrane thickness (Nafion 117)	δ_{mem}	0.23×10^{-3}	m
Catalyst layer thickness	δ_{CL}	0.0287×10^{-3}	m
Anode pressure	P_a	3	atm
Cathode pressure	P_c	3	atm
Inlet fuel and air temperature	T_{cell}	353.15	K
Relative humidity of inlet fuel and air (fully humidified)	ψ	100	%

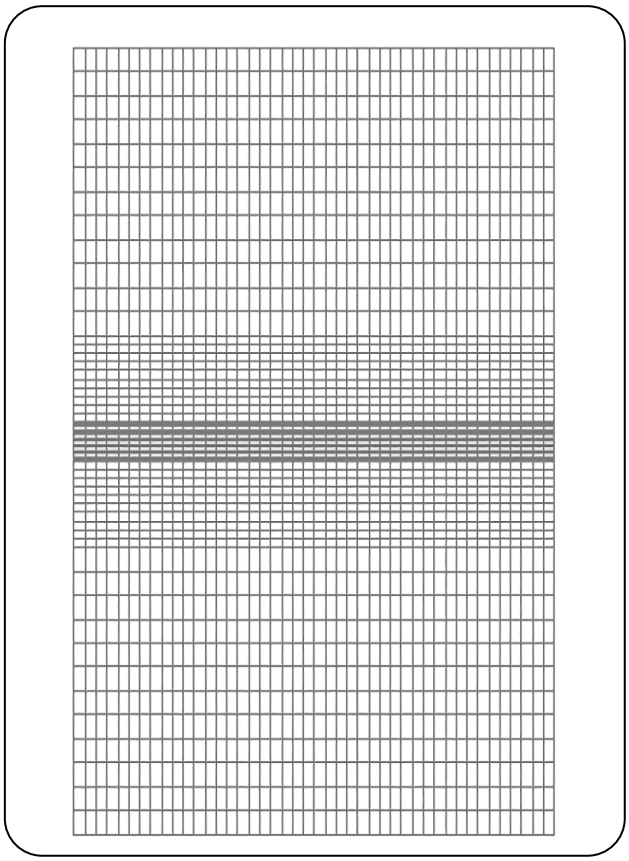

Fig. 4: Grid network of the computational domain.

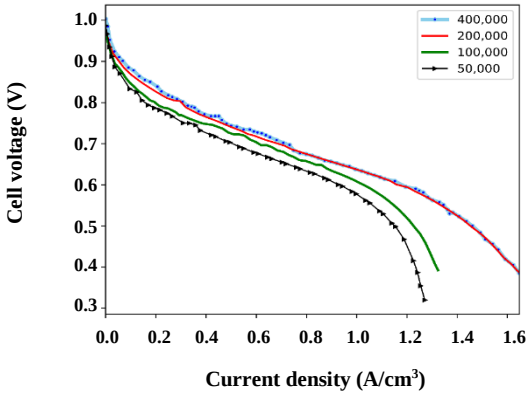

Fig. 5: Grid Independence test of the presented model for polarization diagram.

The present study investigates the effects of geometrical changes on fuel cell outputs. Next, we consider the cylindrical fuel cell model and its ability to improve the cell's operations.

Effects of brand-new designs on polymer fuel cells and the drowning phenomenon

We introduce a new design for cylindrical PEM fuel cells and represent a comparison of operation between this design and the base fuel cell model. We modeled

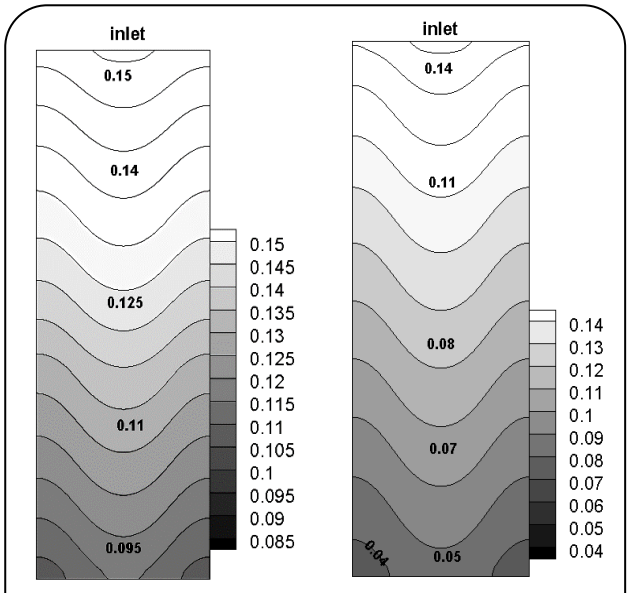

50,000 computational cells 100,000 computational cells

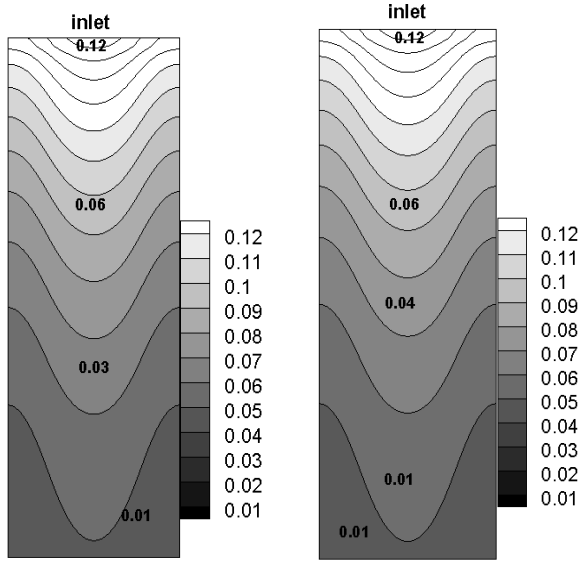

200,000 computational cells 400,000 computational cells

Fig. 6: Oxygen mole fraction in the length of the cathode catalyst layer for the different number of mesh cells.

a cylindrical fuel cell in two elliptical and circular cross-section schemes. The major highlight of this new design is that MEA (Membrane Electrode Assembly) sets in a rectangular form and the cell. Reactional zones are set towards the cell length. We divided these schemes into four subsections: A, B, C, and D (Fig. 7).

The initial design (Case A) has a circular cross-section. We considered the effects of progressive developments in a fuel cell's standard shape in the next section. Case B retains the entire volume of different parts of the fuel cell and transforms it into the elliptical cross-section. To change the circular cross-section to elliptical, the fuel cell shrinks by 20% vertically by keeping the cell components' total volume. While it horizontally extends at the same rate (20%) to keep the total volume constant.

The next section introduces Case C. This Case has a circular cross-section and has the same total volume of MEA as Case A. We should reduce the full fuel cell length to maintain a similar situation. Fig. 8 illustrates the geometrical parameters of cylindrical fuel cells for different cases of this new design of the front view. This unique design retains the total fuel cell volume and MEA constant by increasing the number of channels, electrode sets, and membranes in elliptical and circular cross-sections (Case A, C).

Table 4 demonstrates the dimensional and operational specifications for different cases of Fig. 7. MEA design is observable in Fig. 8 for the presented elliptical and circular cross-sections.

Fig. 9 shows the gas channel schemes of the presented cases.

Fig. 10 displays the comparison of polarization plots of these cases with the base case.

Remarkably, the cylindrical cases generate more outlet current density than the base case. In this approach, Case D produces the maximum and Case A, the minimum current density. Fig. 11 displays the current density distribution contour for the presented cases ($0.4V$).

This development is economically achievable since there is no necessity to set a bump in MEA in this design. This is one of the optimum features of this scheme. It is evident in Fig. 11 that increasing the number of gas channels can increase the outlet's current densities. Considering the shape and the volume of gas channels in cylindrical design, there is the less current density. Fig. 12 shows the velocity rate of reactive gases in anode and cathode gas channels. Increasing the number of channels in elliptical and circular cases increases gas flow velocity. The increment in the number of MEAs leads to an increase in the number of channel inlets. Inlet area decreases in cases, C and A compared to cases B and D.

Accordingly, the reduction in cross-section area leads to a significant decrease in the fluid velocity. Increasing the total channel area leads to an increase in the porous area in the MEA and consequently enhances the speed

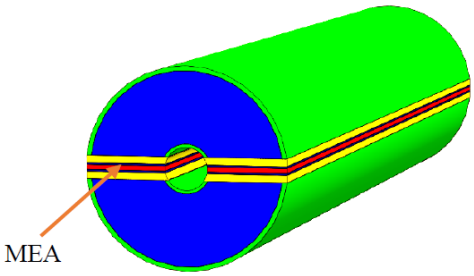

Case A

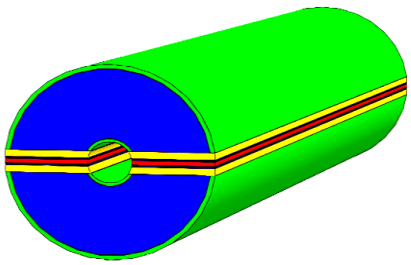

Case B

Case C Case D

Fig. 7: The Three-Dimensional overview of new design.

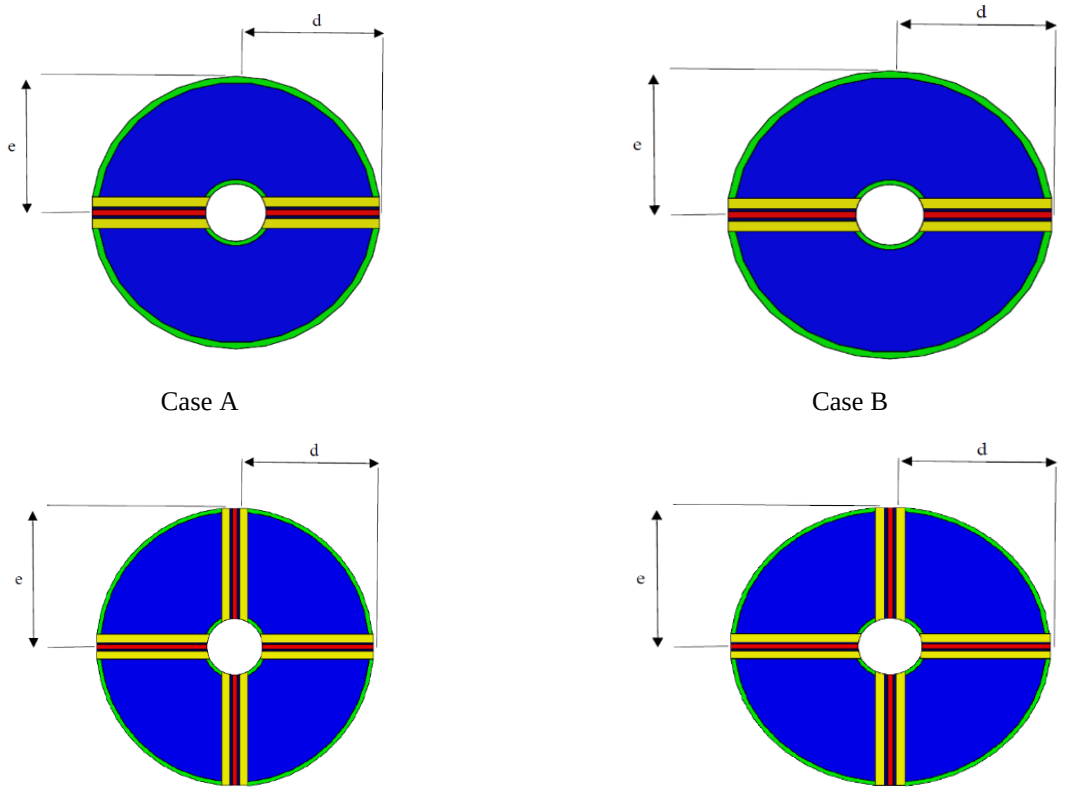

Case A Case B

Case C Case D

Fig. 8: Front view of elliptical, circular and, cylindrical models of fuel cell.

Table 4: Dimensional specifications.

Parameter	Symbol	Units	Case A	Case B	Case C	Case D
Gas channel length	L	mm	42.5	42.5	21.25	21.25
Diffusion layer thickness	δ_{GDL}	mm	0.26	0.26	0.26	0.26
Catalyst layer thickness	δ_{CL}	mm	0.0287	0.0287	0.0287	0.0287
Membrane thickness	δ_{MEM}	mm	0.23	0.23	0.23	0.23
Gas diffusion layer porosity	ϵ_{GDL}	$---$	0.4	0.4	0.4	0.4

Membrane porosity	ε_{MEM}	$---$	0.4	0.4	0.4	0.4
Horizontal Radius	d	mm	2	1.8	2	1.8
Vertical Radius	e	mm	2	2.2	2	2.2
Electrode Effective area	A_{EL}	mm^2	0.000085	0.000085	0.000085	0.000085
The gas Channel Inlet area	A_{ch}	mm^2	2.0865×10^{-6}	1.6844×10^{-6}	1.7081×10^{-6}	2.0643×10^{-6}

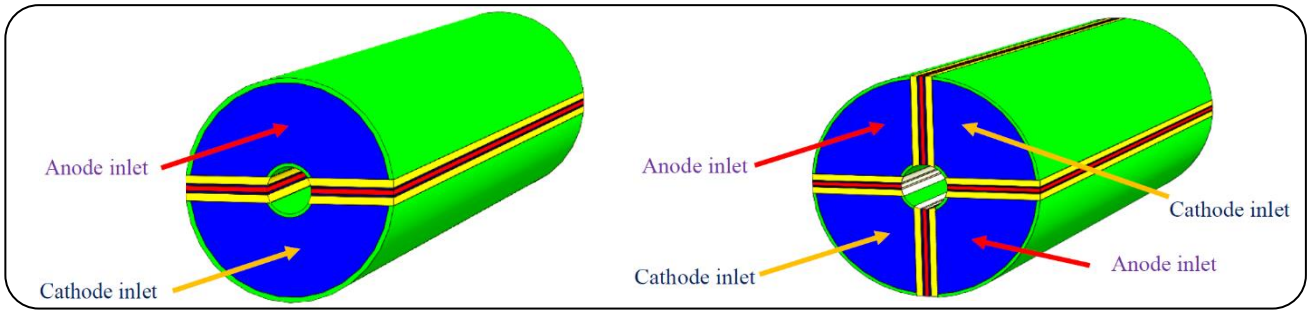

Fig. 9: The Orientation for Gas Flow Entry to Anode and Cathode Channels and Form of Their Composition.

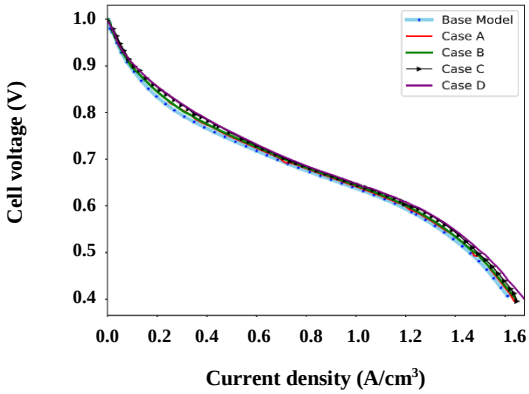

Fig. 10: The comparison of polarization curves for the presented cases.

in cases, C and D. A tense growth in outlet current density is notable in these cases. However, in an elliptical cross-section, a slight increase in the porous area leads to a small boost in current density considering the circular cross-section.

Fig. 13 displays the oxygen mole fraction for the presented cases. Case D has higher oxygen usage than other cases. This Case has the highest output current density and oxygen consumption. On the other hand, Case A has the lowest output current density and the lowest oxygen usage considering other cases.

Fig. 14 displays the water molar concentration for the presented cases on the anode and cathode sides.

Case D has the highest water molar concentration on the cathode side and the lowest rate on the anode side due to water usage. The quantity of water formation in the cathode shows a close connection with fuel cell progression. Thus, increasing fuel cell performance and the output current density increases the water generation. Fig. 14 indicates that water production and water concentration lead

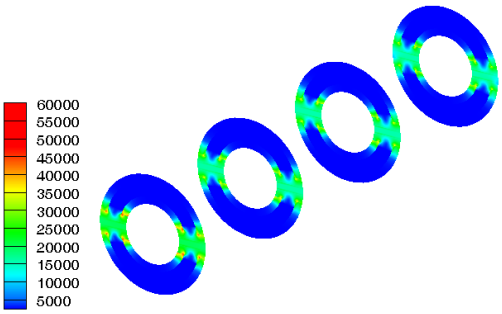

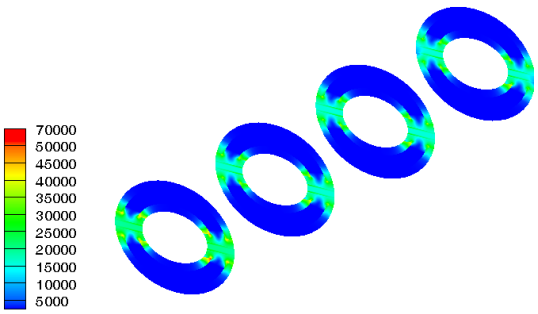

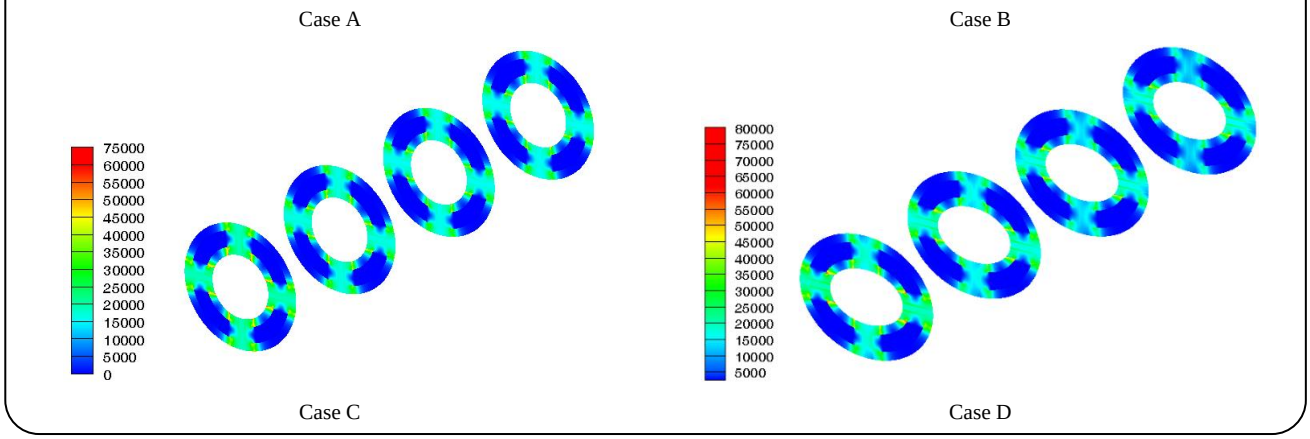

Fig. 11: Comparison of the outlet current density for the presented cases.

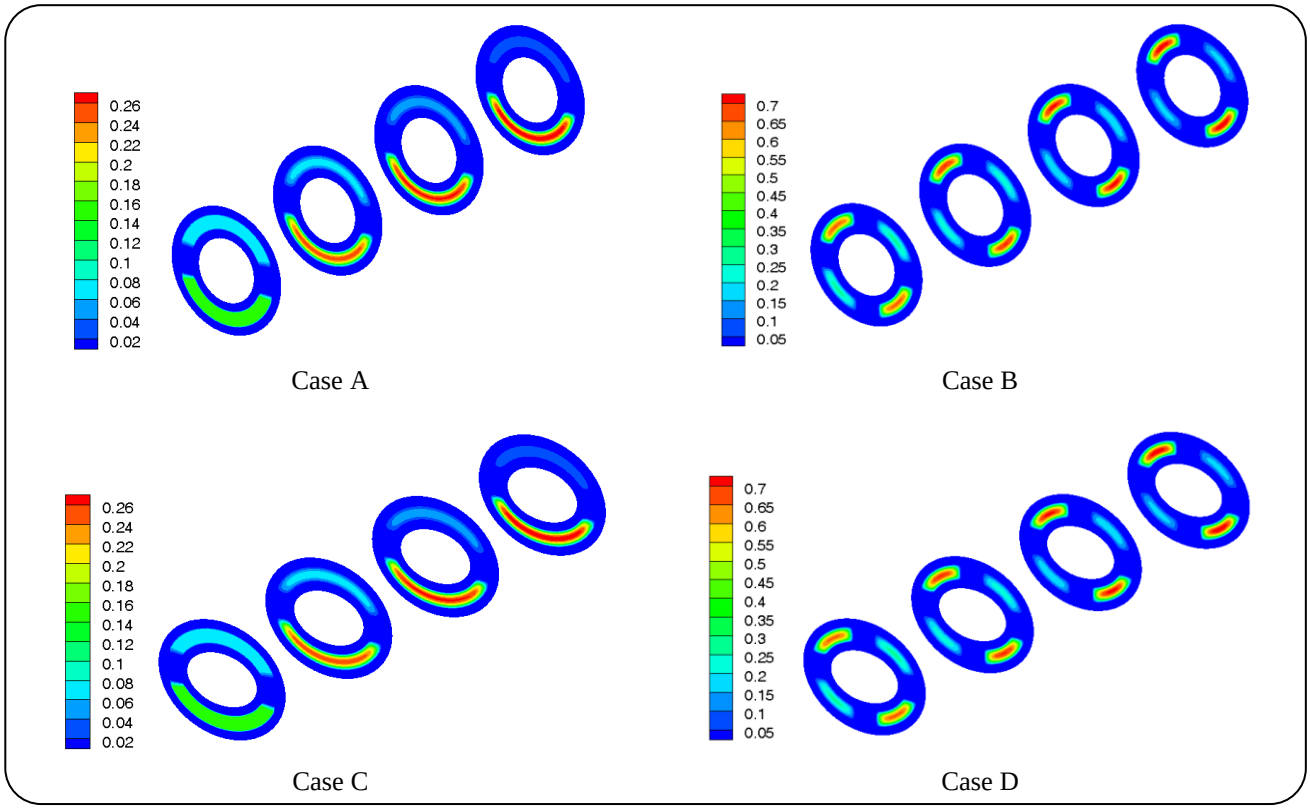

Fig. 12: Comparison of the velocity profiles for the presented cases.

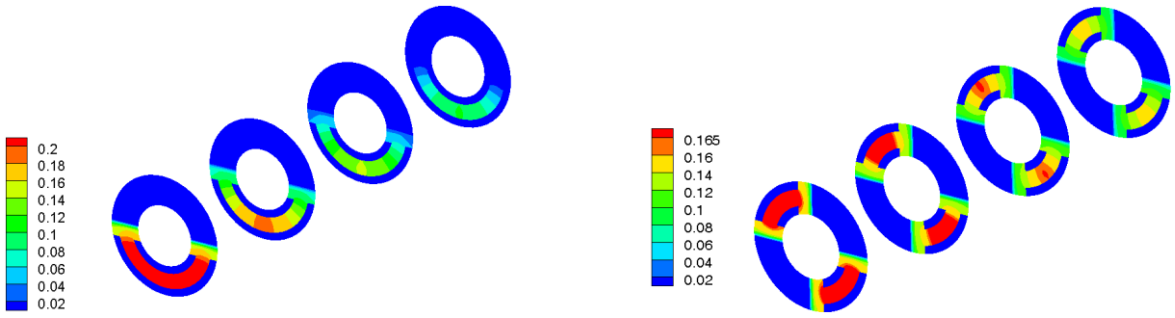

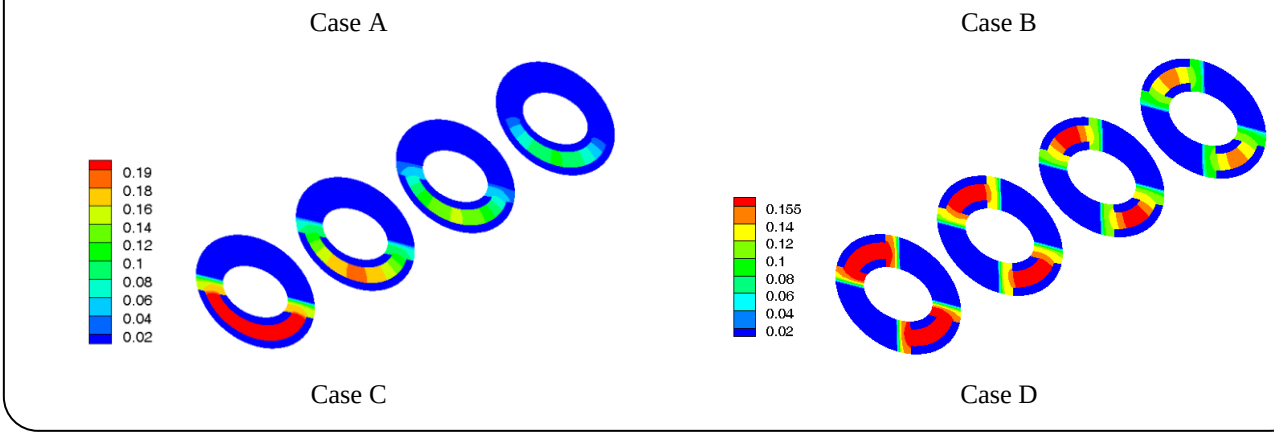

Fig. 13: Comparison of the oxygen mass fraction for the presented cases.

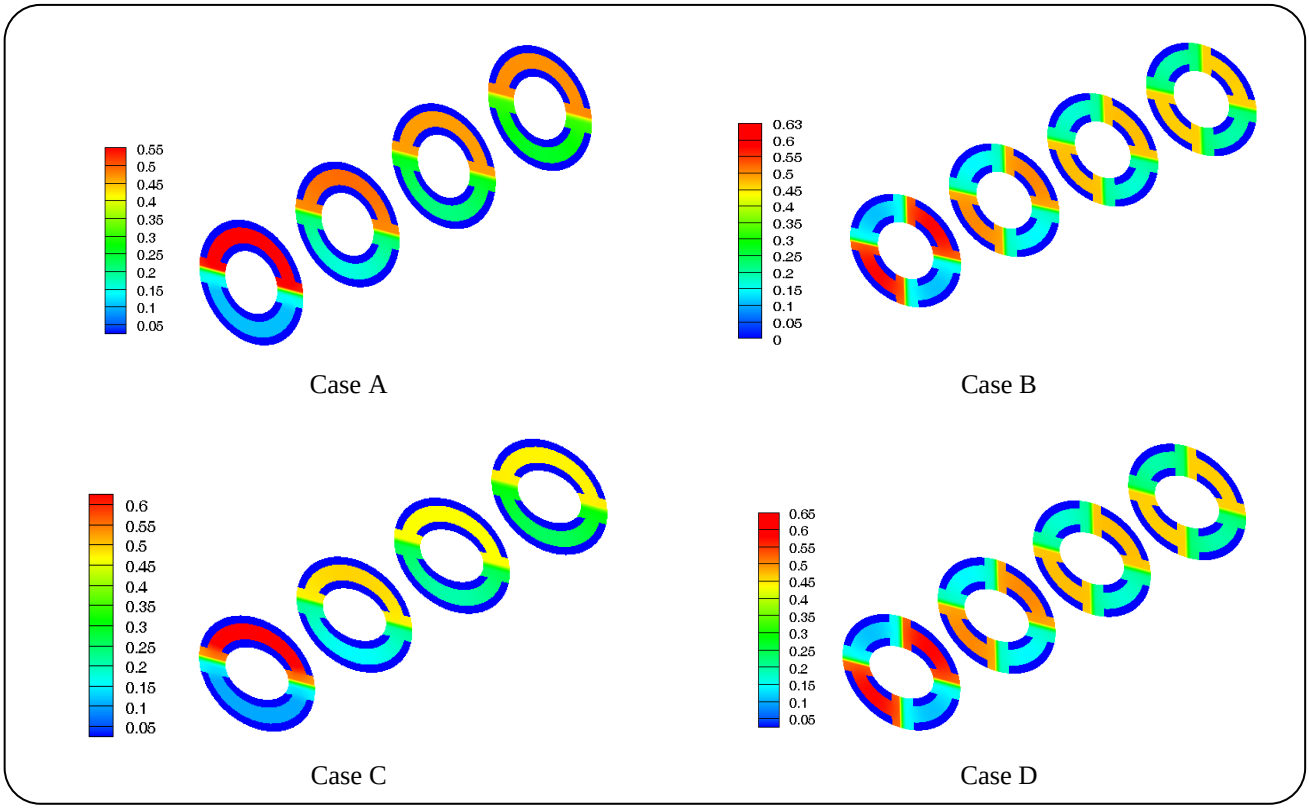

Fig. 14: Comparison of the water mass fraction for the presented cases.

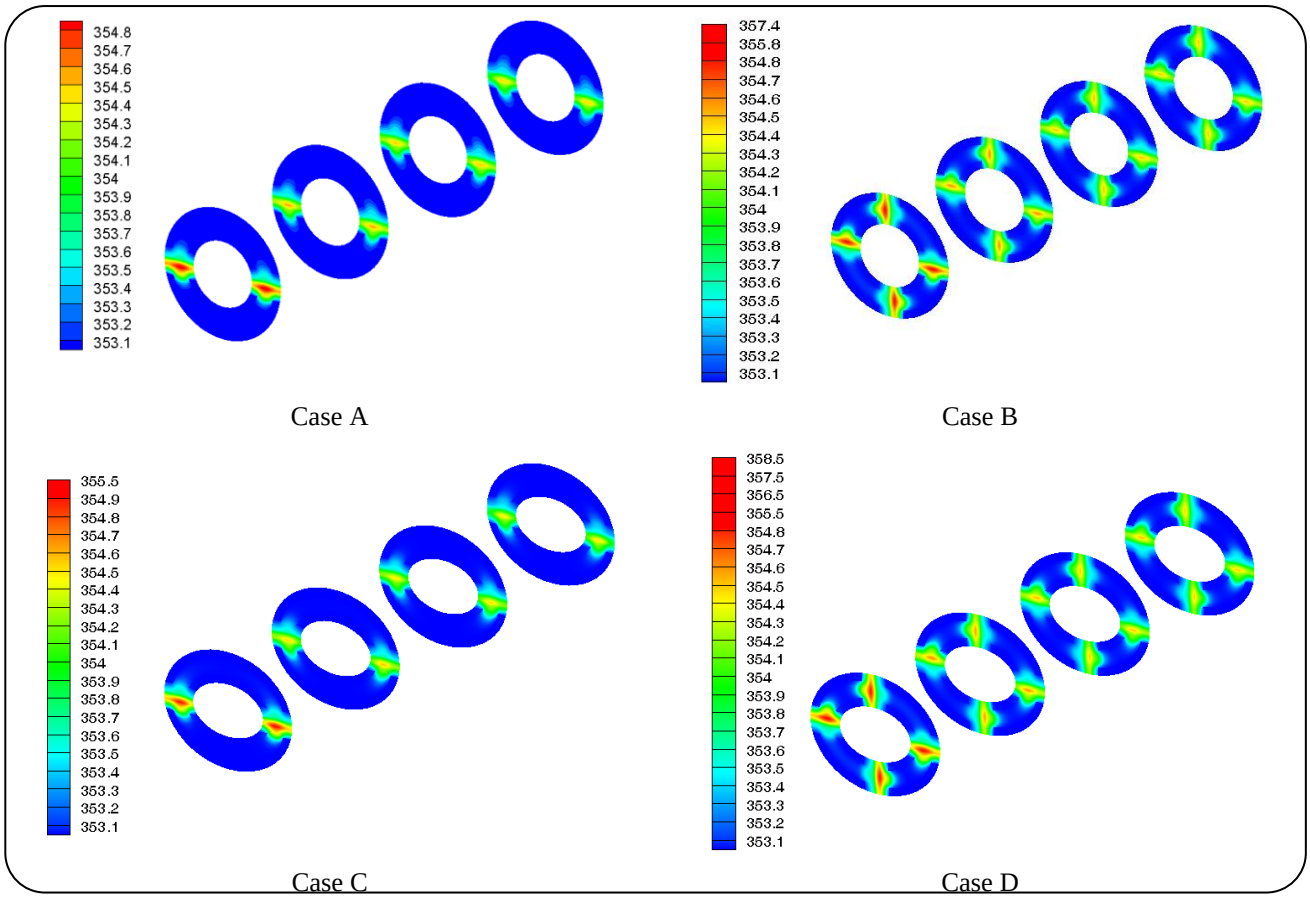

Fig. 15: Comparison of the temperature distribution along with the length of the gas channel for the presented cases.

to a close relation with fuel cell performance. Fig. 15 presents the temperature distribution along with the gas channel length. Cases C and D have higher temperature distribution than other cases. It is due to high intense activity and higher intensity of electrochemical reactions in a fuel cell. Plus, the fuel cell demands a shorter channel length in both of these cases, then the reaction rate is relatively low. Unlike cases C and D, the reaction rate is lower in other cases, and temperature distribution is limited. The amount of the generated current density in the cylindrical case is higher than in the base case.

Fig. 16 displays the amount of liquid water mass fraction toward the new design's channel length. The current density is the ability of the membrane the transportation hydrogen ions to various reaction zones. It is worth noticing that the amount of water density depends on the amount of water in the membrane and the cathode side. In this design, two circumstances cause a higher amount of liquid water mass fraction in the cathode sides. In this brand-new design, firstly, there is a higher amount of formed water in the cathode sides; increasing water accumulation in the cathode section increases liquid water quantity. In this scenario, the chances of water flooding phenomenon increase, especially in lower Voltages. Second, the effective area of the electrode and membrane is relatively low.

Consequently, the water densities in specific regions are considerably high. According to Fig. 16, in both A and B cases, the probability of flooding is substantially increased. If we don't use proper water management, the chances of flooding will rise.

Fig. 17 represents the quantity of pressure drop toward the gas channel; we measured the existing pressure drop as a pressure difference between the inlet and outlet; Cases C and D carry the highest pressure drop value in the channel.

Single-channel designs of cases A and C produce lower pressure drop compared with two previous cases. Two circumstances lead to a higher pressure drop in multi-channel cases. First, the inlet area decreases, and then, the contact region increases in cases A and C. Eventually, the pressure drop in the gas channel increases.

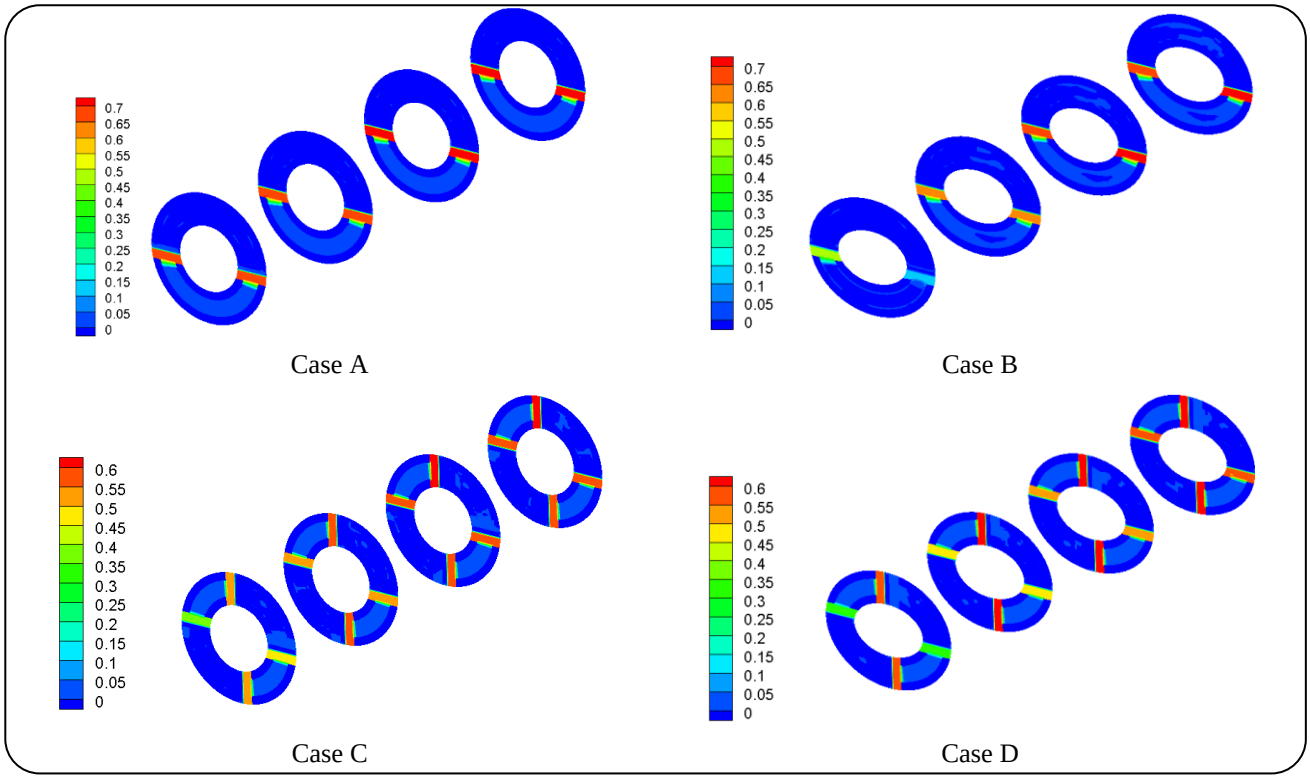

Fig. 16: Comparison of the liquid water mass fraction along with the length of the gas channel for the presented cases.

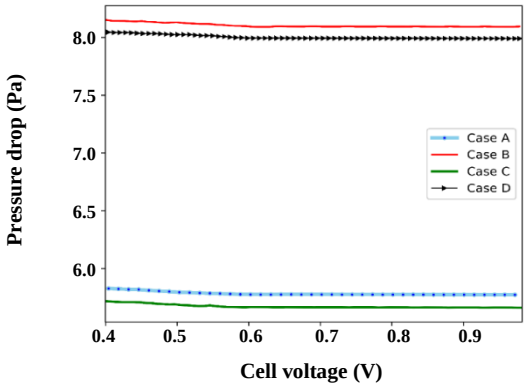

Fig. 17: Comparison of the pressure drop quantity along with the length of the gas channel for the presented cases.

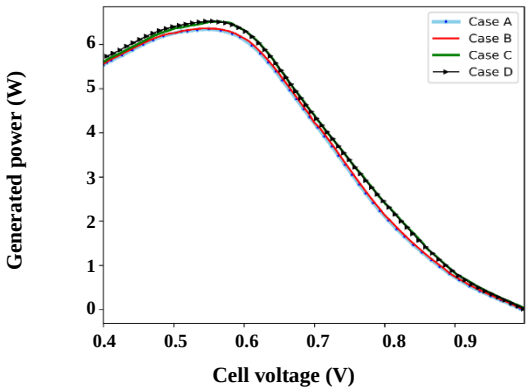

Fig. 18: Comparison of generated power for the presented cases.

The amount of generated power in a fuel cell is obtainable by the following equation:

$$P_{FC} = I \times V \times A_{eff} \quad (15)$$

In Eq. (15), P_{FC} is the generated power. I is the generated current intensity, V cell Voltage generation and A_{eff} is the effective area of the electrode. Fig. 18 denotes the amount of generated power in various Voltages for the presented cases. We measured the amount of generated power by the given Eq. (15). Decreasing the cell voltage will increase the generated power. In Fig. 18, each of the cases, especially Case D, produces the highest power in a range between 0.4V and 0.6V.

The additional required power to offset the pressure drop in channels to pump gases through the channels is achievable *via* the following equation;

$$P_C = \Delta P \times A_{ch} \times u_{in} \quad (16)$$

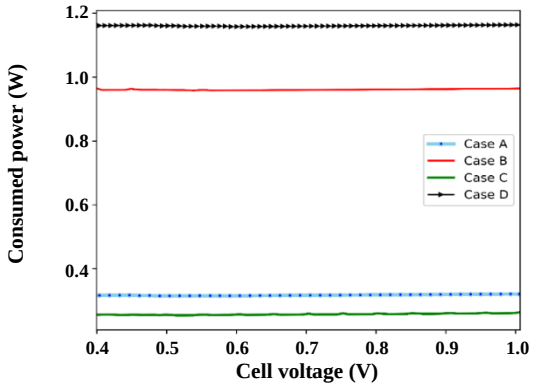

Fig. 19: Comparison of required pumping power for the presented cases.

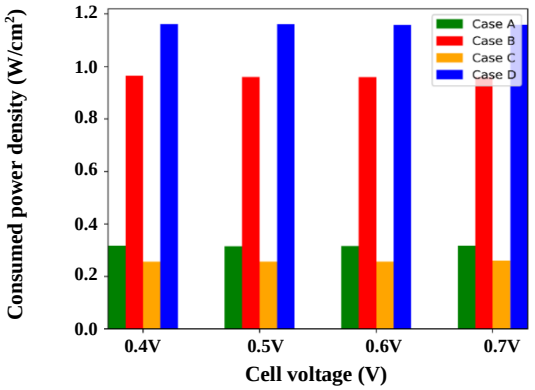

Fig. 20: Comparison of Consumed power density between the presented cases.

In Equation (16), P_c is the extra required pumping power, ΔP is the pressure drop, A_{ch} is the inlet area of the gas channel, and u_{in} is the inlet velocity. In Fig. 19, we presented the extra consumed power to transport gases through the presented cases' channels. Due to the greater inlet area of case D and higher species' velocity, this case's amount of consumed power is higher than in other cases. Case C has the lowest amount of consumed power in all cases.

We designed a new graph for a better demonstration of each of the cases' power consumption, and it is observable in Fig. 20. In this diagram, power consumption for the presented cases is noticeable in four different voltages. In each of these voltages, Case A and Case C have the lowest power usage. Lower power usage means a more economically optimized fuel cell.

CONCLUSIONS

This study presented a Three-Dimensional CFD simulation of the PEM fuel cell with the square-shaped gas channel as a base model. It demonstrates brand-new designs for Polymer Electrolyte Membrane Fuel Cells. Furthermore, we investigated the effects of new schemes on cell functionality and the flooding phenomenon in a fuel cell. These designs are classified into four models called cases A, B, C, and D. Each cylindrical Case generates higher outlet current densities compared with the base case. Among these cases, Case D produces the maximum and Case A, the minimum amount of current density. Increasing the number of channels with fixed volume for elliptical and circular cases results in a boost in gas velocity.

This matter is due to the expansion in the number of Membrane Electrode Assemblies. This process reduces channel inlets for Case C and Case D compared to cases A and B. Accordingly, when the cross-section area reduces at a constant rate, the velocity increases significantly. In the lack of water management, flooding will happen in Case A and Case B. Considering the larger channel inlet area for Case D and its higher species' velocity, the amount of consumed power is higher than in other cases. Case C has the lowest amount of consumed power. We recommend a simulation of a fuel cell using the Lattice Boltzmann Method is for further studies.

Nomenclature

A	Area, m^2
a	Water activity
C	Molar concentration, mol/m^3
D	Mass diffusion coefficient, m^2/s
d	Horizontal Radius of ellipse, mm
e	Vertical Radius of ellipse, mm
F	Faraday constant, C/mol
H	Channel height, m
h	Deflection height, mm
I	Local current density, A/m^2
J	Exchange current density, A/m^2
K	Permeability, m^2
K	Thermal conductivity of gases, W/(m.K)
L	Channel length, m
P	Pressure, Pa
R	Universal gas constant, J/(m.K)
S	Source terms of equations
T	Temperature, K

u	Velocity vector
u	Inlet velocity
W	Width
X	Mole fraction
x	X-direction
y	Y-direction
z	Z-direction
v	Velocity component in the Y direction
w	Velocity component in the Z direction

Greek Letter

ρ	Density, kg/m^3
∇	Vector differential operator
Φ_e	Electrolyte phase potential (-1~1), V
Φ_{sol}	Solid-phase potential, V
Φ_{mem}	Membrane phase potential, V
μ	Viscosity, kg/ m.s
λ	Water content in the membrane
ζ	Stoichiometric ratio
Φ	Electric potential, V
κ	Ion conduction in ion metric phase, S/m
δ	Thickness, m
ψ	Relative humidity, %
ε_{eff}	Effective porosity
w	Water

Subscripts and superscripts

CL	Catalyst Layer
CDL	Gas Diffusion Layer
An	Anode
avg	Average
cat	Cathode
ch	Channel
e	Electrical
in	Inlet
K	Chemical species
MEA	Membrane Electrolyte Assembly
mem	Membrane
sat	Saturation
sol	Solid
eff	Effective

Received : Jul. 13, 2020 ; Accepted : Oct. 26, 2020

REFERENCES

[1] Ahmadi N., Rezazadeh S., Asgharikia M., Shabahangnia E., Optimization of Polymer Electrolyte Membrane Fuel Cell Performance by Geometrical Changes, *Iranian Journal of Chemistry and Chemical Engineering (IJCCE)*, **36(2)**: 89-106 (2017).

[2] T.V. Nguyen, "Modeling Two-Phase Flow in the Porous Electrodes of Proton Exchange Membrane Fuel Cells Using the Interdigitated Flow Fields", *Presented at the 195th Meeting of Electrochemical Society*, 4–7 May, Seattle (1999).

[3] Kilic M.S., Korkut S., Hazer B., Electrical Energy Generation from a Novel Polypropylene Grafted Polyethylene Glycol Based Enzymatic Fuel Cell, *Analytical Letters.*, **47(6)**: 983–995 (2014).

[4] Rezazadeh S., Ahmadi N., Numerical Investigation of Gas Channel Shape Effect on Proton Exchange Membrane Fuel Cell Performance, *Journal of the Brazilian Society of Mechanical Sciences and Engineering*, **37(3)**: 789-802 (2015).

[5] Ahmadi N., Rezazadeh S., Dadvand A., Mirzaee I., Numerical Investigation of the Effect of Gas Diffusion Layer with Semicircular Prominences on Polymer Exchange Membrane Fuel Cell Performance and Species Distribution, *Journal of Renewable Energy and Environment*, **2(2)**: 36-46 (2015).

[6] Chang W.R., Hwang J.J., Weng F.B., Chan S.H., Effect of Clamping Pressure on the Performance of a PEM Fuel Cell, *Journal of Power Sources*, **166(1)**: 149-154 (2007).

[7] Ahmadi N., Taraghi H., Sadeghiazad M., A Numerical Study of a Three-Dimensional Proton Exchange Membrane Fuel Cell (PEMFC) with Parallel and Counter Flow Gas Channels, *Iranian Journal of Science and Technology, Transactions of Mechanical Engineering*, **39**: 309-323 (2015).

[8] Amphlett J.C., Baumert R.M., Mann R.F., Peppley B.A., Roberge P.R., Harris T.J., Performance Modeling of the Ballard Mark IV Solid Polymer Electrolyte Fuel Cell. I. Empirical Model Development, *J. Electrochem. Soc.*, **142**: 9-15 (1995).

[9] Werner C., Busemeyer L., Kallo J., The Impact of Operating Parameters and System Architecture on the Water Management of a Multifunctional PEMFC System, *International Journal of Hydrogen Energy* (2015).

[10] Kwon O.-J., Shin H.-S., Cheon S.-H., Oh B.S., A Study of Numerical Analysis for PEMFC Using a Multiphysics Program and Statistical Method, *International Journal of Hydrogen Energy*, **40(35)**: 11577-11586 (2015).

[11] Lee D., Lim J.W., Nam S., Choi I., Lee D.G., Gasket-Integrated Carbon/Silicone Elastomer Composite Bipolar Plate for High-Temperature PEMFC, *Composite Structures*, **128**: 284-290 (2015).

[12] Uribe F.A., Gottesfeld S., Zawodzinski T.A., Effect of Ammonia as Potential Fuel Impurity on Proton Exchange Membrane Fuel Cell Performance, *J. Electrochem. Soc.*, **149**: A293-A296 (2002).

[13] Ticianelli E.A., Derouin C.R., Srinivasan S., Localization of Platinum in Low Catalyst Loading Electrodes to Attain High Power Densities in SPE Fuel Cells, *J. Electro anal. Chem.*, **251**: 275–295 (1988).

[14] Yao K.Z., Karan K., McAuley K.B., Oosthuizen P., Peppley B., Xie T., A Review of Mathematical Models for Hydrogen and Direct Methanol Polymer Electrolyte Membrane Fuel Cells, *Fuel Cells*, **4(1/2)**: 3–29 (2004).

[15] Natarajan D., Nguyen T.V., A Two-Dimensional, Two-Phase, Multi-Component, Transient Model for the Cathode of a Proton Exchange Membrane Fuel Cell Using Conventional Gas Distributors, *J. Electrochem.Soc.*, **148(12)**: A1324–A1335 (2001).

[16] Ahmadi N., Rezazadeh S., Yekani M., Fakouri, A., Mirzaee I., Numerical Investigation of the Effect of Inlet Gases Humidity on Polymer Exchange Membrane Fuel Cell (PEMFC) Performance, *Transactions of the Canadian Society for Mechanical Engineering*, **37(1)**: 1-20 (2013).

[17] Lum K.W., McGuirk J.J., Three-Dimensional Model of a Complete Polymer Electrolyte Membrane Fuel Cell-Model Formulation, Validation, and Parametric Studies, *J. Power Source.*, **143**: 103–124 (2005).

[18] Ahmed D.H., Sung H.J., Effects of Channel Geometrical Configuration and Shoulder Width on PEMFC Performance at High Current Density, *J. Power Source.*, **162**: 327–339 (2006).

[19] Ahmadi N., Dadvand A., Rezazadeh S., Mirzaee I., Analysis of the Operating Pressure and GDL Geometrical Configuration Effect on PEM Fuel Cell Performance, *Journal of the Brazilian Society of Mechanical Sciences and Engineering*, **38(8)**: 2311-2325 (2016).

[20] Ebrahimi S., Roshandel R., Vijayaraghavan K., Power Density Optimization of PEMFC Cathode with Non-Uniform Catalyst Layer by Simplex Method and Numerical Simulation, *International Journal of Hydrogen Energy*, **41(47)**: 22260-22273 (2016).

[21] Cooper N.J., Santamaria A.D., Becton M.K., Park J.W., Investigation of the Performance Improvement in Decreasing Aspect Ratio Interdigitated Flow Field PEMFCs, *Energy Conversion and Management*, **136**: 307-317 (2017).

[22] Yan W.M., Li H.Y., Weng W.C., Transient Mass Transport and Cell Performance of a PEM Fuel Cell, *International Journal of Heat and Mass Transfer*, **107**: 646-656 (2017).

[23] Liu J.X., Guo H., Ye F., Ma C.F., A Two-Dimensional Analytical Model of a Proton Exchange Membrane Fuel Cell, *Energy*, **119**: 299-308 (2017).

[24] Ahmadi N., Dadvand A., Mirzaei I., Rezazadeh S., Modeling of Polymer Electrolyte Membrane Fuel Cell with Circular and Elliptical Cross- Section Gas Channels: A Novel Procedure, *International Journal of Energy Research*, **42(8)**: 2805-2822 (2018).

[25] Ahmadi N., Rezazadeh S., Dadvand A., Mirzaee I., Modeling of Gas Transport in Proton Exchange Membrane Fuel Cells, *Proceedings of the Institution of Civil Engineers-Energy*, **170(4)**: 163-179 (2016).

[26] Garau V., Liu H., Kakac S., Two-Dimensional Model for Proton Exchange Membrane Fuel Cells, *AIChE J.*, **44(11)**: 2410-2422 (1998).

[27] Meredith R.E., Tobias C.W., Phenomena and Effects of Electrolytic Gas Evolution, "Advances in Electrochemistry and Electrochemical Engineering", (Tobias, C.W., ed., Interscience Publishers, New York, (1960)).

[28] Byron Bird R., Warren E. Stewart, Edwin N. Lightfoot, "Transport Phenomena", John Wiley & Sons, Inc, (1960)

[29] Springer T.E., Zawodzinski T.A., Gottesfeld S., Polymer Electrolyte Fuel Cell Model, *J. Electrochem. Soc.*, **138**: 334-2342 (1991).

[30] Kuklikovsky A.A., Quasi-3D Modeling of Water Transport in Polymer Electrolyte Fuel Cells, *J. Electrochem. Soc.*, **150(11)**: A1432-A1439 (2003).

[31] Meredith R.E., Tobias C.W.,"Advances in Electrochemistry and Electrochemical Engineering 2", Tobias, C.W. (ed.), Interscience Publishers, New York, (1960).

[32] Yeo S.W., Eisenberg A., Physical Properties and Super-Molecular Structure of Perfluorinated Ion-Containing (Nafion) Polymers, *J. Appl. Polym. Sci.*, **21**: 875-898 (1977).

[33] Springer T.E., Zawodinski T.A., Gottesfeld S., Polymer Electrolyte Fuel Cell Model, *J. Electrochem. Soc.*, **136**: 2334-2342 (1991).

[34] Wang L., Husar A., Zhou T., Liu H., A Parametric Study of PEM Fuel Cell Performances, *J. Hydrog. Energy*, **28**: 1263-1272 (2003).

[35] Ahmadi N., Kõrgesaar M., Analytical Approach to Investigate the Effect of Gas Channel Draft Angle on the Performance of PEMFC and Species Distribution, *International Journal of Heat and Mass Transfer*, **152**: 119529 (2020).